Research Article

Rapid Communications in Mass Spectrometry

Received: 15 November 2016 Revised: 12 January 2017 Accepted: 6 February 2017 Published online in Wiley Online Library

Rapid Commun. Mass Spectrom. **2017**, *31*, 674–684
(wileyonlinelibrary.com) DOI: 10.1002/rcm.7836

Two-dimensional mass spectrometry in a linear ion trap, an *in silico* model

Maria A. van Agthoven and Peter B. O'Connor*

Department of Chemistry, University of Warwick, Gibbet Hill Road, Coventry CV4 7AL, UK

RATIONALE: Two-dimensional mass spectrometry (2D MS) is a technique that correlates precursor and product ions in a sample without requiring prior ion isolation. Until now, this technique has only been implemented on Fourier transform ion cyclotron resonance mass spectrometers. By coupling 2D MS techniques in linear ion traps (LITs) with a mass analyser with a fast duty cycle (e.g. time-of-flight), data-independent tandem mass spectrometry techniques can be compatible on a liquid chromatography (LC) or gas chromatography (GC) timescale.
METHODS: The feasibility of 2D MS in a LIT is explored using SIMION ion trajectory calculations.
RESULTS: By applying stored waveform inverse Fourier transform techniques for radial excitation on a LIT, the sizes of ion clouds were found to be modulated according to the ions' resonant frequencies in the LIT. By simulating a laser-based fragmentation at the centre of the LIT after the radius modulation step, product ion abundances were found to be modulated according to the resonant frequency of their precursor.
CONCLUSIONS: A 2D mass spectrum could be obtained using the results from the simulation. This *in silico* model shows the feasibility of 2D MS on a LIT. 2D MS in a LIT allows for tandem mass spectrometry without ion isolation.

Two-dimensional mass spectrometry (2D MS) is a technique that correlates precursor and product ions in a sample without requiring prior ion isolation. 2D MS was first proposed by Pfändler *et al.* in 1987[1–3] on a Fourier transform ion cyclotron resonance (FT-ICR) mass spectrometer.[4] The pulse sequence for 2D MS was inspired both by NOESY NMR spectroscopy[5] and by phase-reversion experiments performed by Marshall *et al.*[6] Using two identical excitation pulses separated by a regularly incremented delay, ion cyclotron radii are modulated according to their cyclotron frequency (i.e. mass-to-charge ratio) before a fragmentation period with a radius-dependent fragmentation method.[7] The resulting 2D mass spectrum shows the fragmentation patterns of all ions from the sample, which enables easy extraction of product ion scans, precursor ion scans and neutral loss lines, as well as electron capture lines.[8] Since 2D mass spectra show the fragmentation patterns of all ions from a sample without requiring ion isolation, this technique can be said to be truly data-independent and can be of great use for the analysis of complex samples.

Since 2010, thanks to improvements in computational capacities for data processing and storage, 2D MS on FT-ICR instruments has been developed into a fully-fledged analytical technique with infrared multiphoton dissociation (IRMPD) and electron capture dissociation (ECD) as fragmentation methods.[9–11] De-noising algorithms have been developed in order to reduce the effects of scintillation noise in 2D mass spectra.[12,13] 2D MS has been successfully applied to the analysis of small molecules[14] as well as in bottom-up[15,16] and top-down proteomics.[17] In 2D MS, the correlation between precursor ions and their products is fully multiplexed, which enables the differentiation, for example, of product ion patterns between two precursor ion species with different charge states but with overlapping isotopic distributions.[16] Furthermore, because 2D MS is based on Fourier transformation in both dimensions, the signal-to-noise ratio and the resolving power of 2D mass spectra both increase with the number of data points.

Other data-independent acquisition techniques include Precursor acquisition independent from ion count (PAcIFIC),[18,19] Sequential Window Acquisition of all THeoretical fragment ion spectra (SWATH),[20] and MS^E.[21] PAcIFIC and SWATH consist of scanning the isolation window with tandem mass spectrometry (MS/MS). MS^E takes advantage of the rapid duty cycle of quadrupole/time-of-flight (QTOF) analysers and consists of acquiring an MS spectrum, a low collision energy MS/MS spectrum and a high collision energy MS/MS spectrum at each retention time without ion isolation with online liquid chromatography. Recently, MS^E has also been applied to electron transfer dissociation (MS^{ETD}).[22] With MS^E, precursor and product ions cannot be correlated accurately if multiple precursors co-elute. PAcIFIC and SWATH rely on narrow or wide-band isolations, respectively, of precursors in *m/z* using the quadrupole mass filter, and, similarly, it is not possible to determine directly which product comes from which precursor if they are in the same isolation window. However, PAcIFIC, SWATH, and MS^E can be applied to a large number of mass analysers, whereas 2D MS has so far been confined to FT-ICR mass analysers.

* *Correspondence to:* P. B. O'Connor, Department of Chemistry, University of Warwick, Gibbet Hill Road, Coventry CV4 7AL, UK.
E-mail: p.oconnor@warwick.ac.uk

Rapid Communications in Mass Spectrometry

Although most FT-ICR mass spectrometers use frequency-swept excitation, an alternative method to generate excitation pulses is the stored waveform inverse Fourier transform (SWIFT) technique.[23–26] SWIFT has been used for high-resolution ion isolation[27,28] as well as for multiplexed MS/MS using Hadamard transformation.[29–32] In 1993, Ross *et al.* used SWIFT to develop an alternative pulse sequence for 2D MS on an FT-ICR mass spectrometer.[33] Instead of using delays between pulses, this pulse sequence uses the fact that the cyclotron radius of an ion after excitation is proportional to the product of the excitation amplitude and the excitation length.[34] Excitation pulses are generated with amplitudes that are modulated according to the excitation frequency. Applying these excitation pulses to precursor ions in the ICR cell modulates their cyclotron radii according to their cyclotron frequencies and therefore modulates the abundances of their products after radius-dependent fragmentation. This technique, called stored waveform ion radius modulation (SWIM), was applied to the analysis of amino acid dimers and trimers[35] and to the analysis of polymers and pharmaceutical products.[36] However, because SWIFT is not available on most commercial FT-ICR instruments, the original pulse sequence for 2D FT-ICR MS is easier to use than SWIM.[8]

Although 2D MS shows good results on FT-ICR instruments, its development is hampered by the fact that FT-ICR instruments are expensive to purchase and maintain. Furthermore, due to the duty cycle of the FT-ICR mass spectrometer, each 2D MS experiment can take 30 min or more. Developing 2D MS techniques that can be applied to other mass spectrometers is therefore important for the development of data-independent structural analysis of complex samples. There have been some developments in this direction. Yoon *et al.* have designed fragmentation modulation mass spectrometry (FMMS) for TOF-MS by modulating the efficiency of a fragmentation mode in interaction with ion beams.[37] Vachet and coworkers have used the low-mass cut-off in the ion injection of quadrupolar ion traps and rectilinear ion traps to modulate precursor and product ion intensities.[38,39]

Linear ion traps (LITs)[40] are popular ion manipulation devices. Their dimensions allow for larger ion populations than quadrupolar ion traps.[41] Resonant mass-selective radial excitation is well established with LITs.[42,43] SWIFT excitation has been developed for quadrupolar ion traps and can reasonably be applied to LITs.[25,44,45] In addition to requiring far less stringent timing accuracy, the advantage of SWIM is that, unlike the original 2D FT-ICR pulse sequence, the radial modulation does not require the ion cloud to be coherent. If the overlap between the density of an ion species and the fragmentation zone can be modulated using SWIM, then product ion abundances can be modulated according to the resonant frequencies of their precursors, which then enables 2D MS in a LIT. In a LIT, all ions have a resonant 'secular frequency' in the pseudopotential well, which can be used to modulate the precursor ion cloud size radially using SWIM.[41]

In this study, the feasibility of 2D MS in a LIT is explored using SIMION ion trajectory calculations. The proposed setup for 2D MS in a LIT is outlined in Scheme 1. An ion source, a quadrupole with two end-cap electrodes and the necessary equipment for fragmentation in the quadrupole (for instance, a laser for photodissociation) comprise the equipment for the experiment. The ions are stored in the quadrupole by applying a direct current (DC) trapping potential on the end-cap electrodes and a radiofrequency (RF) voltage on the quadrupole rods. The SWIM pulse is added to the RF voltage in order to increase the radius of ion trajectories in the quadrupole. The fragmentation mode is then applied and ions at the centre of the quadrupole are preferentially fragmented. This setup allows for the analysis of positive or negative ions only. Applying RF end-cap voltages would allow the analysis of negative and positive ions simultaneously.

SIMULATION METHODS

Electrode geometry design

All simulations were performed using SIMION 8.0 (Scientific Instrument Services, Ringoes, NJ, USA) on an ion optic bench with the following dimensions: x = 16 mm, y = 16 mm, z = 83 mm. The linear ion trap (LIT) was built in a single potential array with a mirror symmetry around the y = 0 plane and is similar to the one modelled by Schwartz *et al.*[40]

The potential array contained 11 electrodes with a 10 grid unit/mm precision and was refined with a convergence limit of 10^{-5}. Figure 1 shows the ion optics bench containing the LIT.

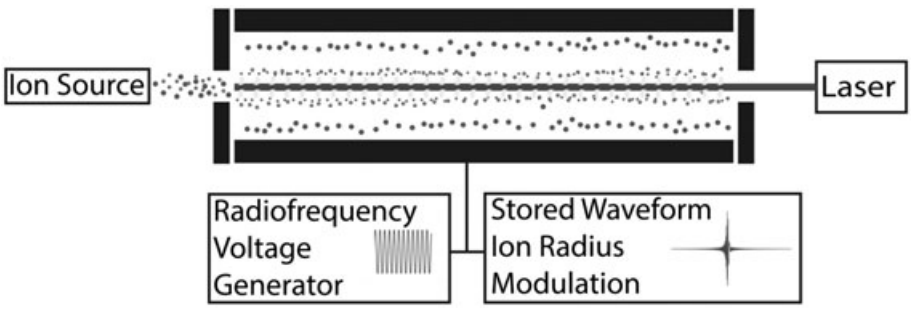

Scheme 1. Setup for two-dimensional mass spectrometry in a linear ion trap. SWIM pulses are added to the RF drive voltage to preferentially excite some precursors to high radius in the LIT. Precursors remaining at low radius are fragmented by radius-dependent fragmentation methods such as IRMPD, ETD, CID (continuous fragmentation) or UVPD (pulsed fragmentation).

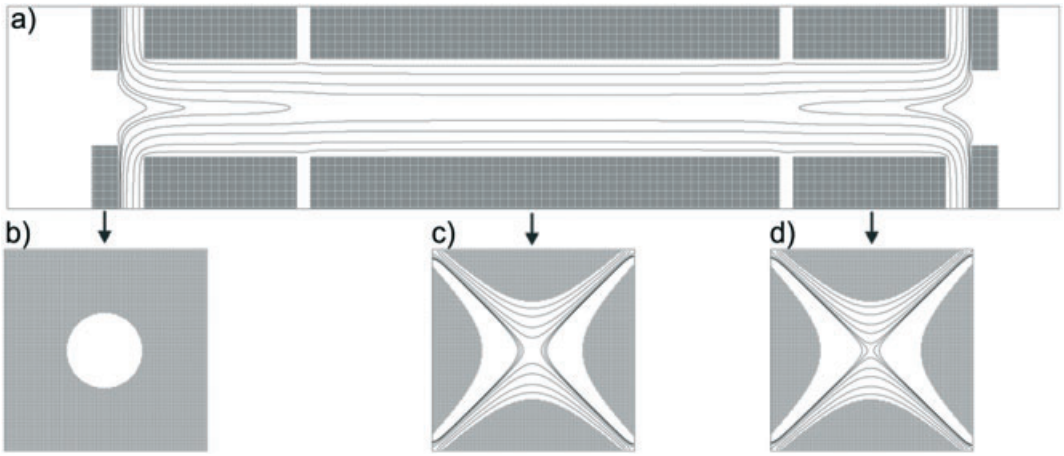

Figure 1. SIMION model of the linear ion trap with equipotential lines: (a) horizontal cut; (b) vertical cut of trapping electrode; (c) vertical cut of centre quadrupole; and (d) vertical cut of side quadrupole. The voltages applied on the LIT electrodes in this instance are +10.0 V_{DC} on the end-cap electrodes, +5.0 V_{DC} on the outer quadrupole rods, ±100.0 V_{RF} on the quadrupole rods. The equipotential lines are for: –100.0 V, –75.0 V, –50.0 V, –25.0 V, –10.0 V, 0.0 V, +2.5 V, +5.0 V, and +10.0 V.

Figure 1(a) shows that two end-caps are used to contain ions axially and three quadrupoles are used to contain ions radially. The centre quadrupole is RF-only and is used to apply the RF trapping voltage and the SWIM pulse. The two outer quadrupoles are used to apply the RF trapping voltage and a DC axial trapping voltage that is half the DC voltage on the end-cap electrodes. Figure 1(b) shows the end-cap electrodes: their thickness is 2 mm and their opening has a 3 mm radius. They are separated from the quadrupoles by a 2 mm gap. Figures 1(c) and 1(d) show that the quadrupole rods are hyperbolically shaped with an internal radius of 4 mm. The length of the outer quadrupoles is 12 mm. The length of the centre quadrupole is 37 mm. The quadrupoles are separated by a 1 mm gap.

Experimental script

Scheme 2 shows the experimental script used to simulate ion trajectories. The workbench program used in order to generate the experimental conditions was written in Lua

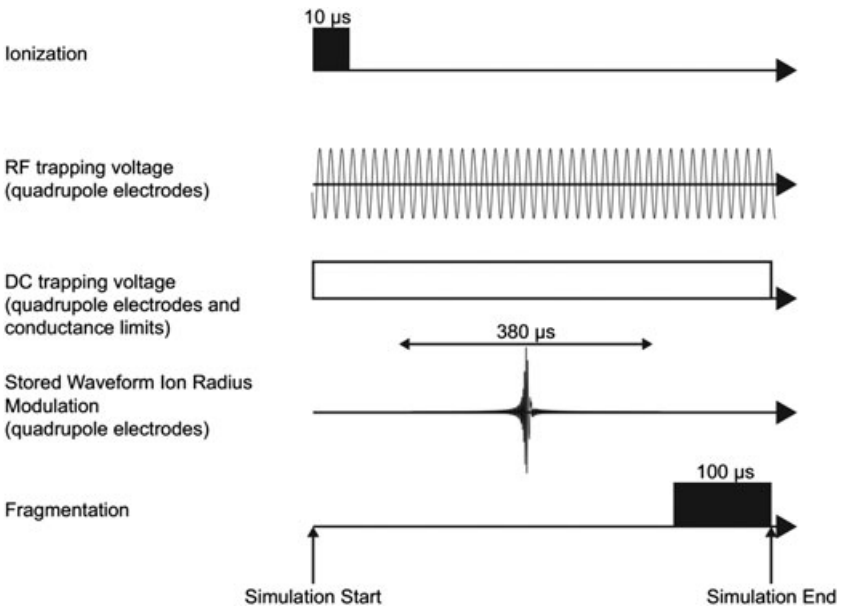

Scheme 2. Experimental sequence of the 2D simulation corresponding to the SIMION program. The ionisation is programmed in the segment.initialize() function of the workbench program, the trapping voltages and SWIM voltages are programmed in the segment.fast_adjust() function, and the fragmentation is programmed in the segment.other_action() function (see Supporting Information).

Rapid Communications in Mass Spectrometry

5.1.1 (Rio de Janeiro, Brazil) programming language and can be found in the Supporting Information. Ionisation was randomised in an area with a 0.2 mm radius in the middle of the LIT during the first 10 µs of each ion trajectory simulation (initialise segment). The continuous trapping voltages were set at +10.0 V on the end-cap electrodes and +5.0 V on the rods of the outer quadrupoles throughout the ion trajectory simulation. An RF voltage with a 300.0 V_{pp} amplitude and a 1.1 MHz frequency was applied to all three quadrupoles.

After 50.0 µs, an excitation pulse generated externally using SWIFT was applied to the rods of the centre quadrupole with a 700-fold gain and a 20–550 kHz frequency range (*vide infra*) in addition to the RF drive voltage. The SWIM excitation pulses, calculated from a frequency envelope with a maximum amplitude of 1 (arbitrary unit), had a maximum of about 0.1 in the time domain (zero-to-peak, arbitrary unit). The maximum amplitude of the resulting voltage after multiplication of the values in the SWIM pulse by the gain was about 70 $V_{zero\text{-}to\text{-}peak}$. The highest frequency of this range was chosen to be half the drive frequency and corresponds to the limit of stability in the Mathieu stability diagram.[41] The lowest frequency of this range was chosen in order to enable the excitation over a mass range of approximately *m/z* 120–1500. The length of each pulse was set at 380 µs (fast_adjust segment). The SWIM pulses were *de facto* synchronised with the RF drive voltage, but the effects of this synchronisation were not studied. In order to ensure that the time step of the ion trajectory simulation was constant for the application of the excitation pulse, the TQual parameter in the ion optics bench was set at 0 and the time step was set at 10 ns (tstep_adjust segment). At the end of the excitation pulse, a fragmentation period was modelled using a top-hat distribution fragmentation zone with a 0.05 mm radius. The probability of fragmentation was calculated using the following equation:

$$P = 1 - e^{-\frac{t}{T_{decay}}} \quad (1)$$

in which P is the probability of fragmentation, t the time that the ion has spent within the fragmentation zone during the fragmentation period and T_{decay} was set at 500.0 µs. This model was chosen in order to mimic a laser-based fragmentation method. Both the radius of the fragmentation zone and the time decay were chosen arbitrarily in order to result in reasonable fragmentation efficiency. The effect of this choice will be discussed below. Only one fragmentation was allowed during each ion trajectory simulation. After the fragmentation period the ion trajectory calculation was set to end (other_actions segment). The experimental script was repeated 128 times with 128 different excitation pulses.

SWIM pulse generation

128 stored waveform ion radius modulation (SWIM) pulses were generated using python 2.7 programming language in the Spyder 2.3.8 development environment (Anaconda, Continuum Analytics, Austin, TX, USA) and stored in a Comma Separated Values (csv) file format in order to be called by the SIMION workbench program. The SWIM pulse generation program is listed in the Supporting Information. Scheme 3 summarizes the process of generating each pulse, as proposed by Ross *et al*.[33,36] The frequency range of each pulse is 20–2117.151 kHz, but the amplitude of each pulse is non-zero over a 20–550 kHz frequency range. The frequency increment was 1 Hz. The amplitude envelope of each pulse is determined by the following equation:

$$M_{(f,n)} = \frac{1}{2}\left(1 + \sin\left(n\pi\left(\frac{f - f_{min}}{f_{max} - f_{min}}\right) - \frac{1}{2}\right)\right) \quad (2)$$

in which M is the amplitude, f the frequency, n the index of the pulse, f_{max} the maximum frequency of the pulse (here, 550 kHz) and f_{min} the minimum frequency of the pulse (here, 20 kHz). In order to reduce the maximum voltage of the time-domain pulse, a quadratic phase function as proposed by Guan and McIver[26] was applied to the frequency-domain pulse:

$$\varphi_{(f)} = \frac{\pi}{20}\frac{(f - f_{min})^2}{f_{max,range} - f_{min}} \quad (3)$$

in which φ is the phase, f the frequency, $f_{max,range}$ the maximum frequency of the total frequency range (here, 2117.151 kHz) and f_{min} the minimum frequency (here, 20 kHz). The resulting function, combining Eqns. (2) and (3):

$$PM_{(f,n)} = M_{(f,n)} \times e^{i\varphi_{(f)}} \quad (4)$$

was transformed into a time-domain pulse using the real part of its inverse fast Fourier transform.

The resulting time-domain pulse was 1 s long with a 0.477 µs sampling period. The significant part of the pulse was truncated to 380 µs and interpolated in order to achieve a 10 ns time increment before storage in a csv file. As a result, the time increment of the SWIM pulses coincided with the time increment of the ion trajectory simulations.

Particle definition, data recording, and data processing

Ion trajectory calculations were run without Coulombic repulsion or collisions with a background gas. For each SWIM pulse, the trajectory of 100 ions of *m/z* 166, 195, and 322 were calculated. The *m/z* values of their products were *m/z* 122, 181, and 190, respectively. All *m/z* values were chosen arbitrarily. For each ion trajectory calculation, the index, *m/z* value and time-of-flight of the ion were recorded and stored in a text file at the moment of ion splat or the end of the simulation. The total ion current (TIC) was defined as the number of ions still present in the LIT at the end of the simulation.

Using the Python 2.7 programming language, the data recorded from the ion trajectory calculations was converted into a 2D mass spectrum. For each *m/z* value, the Fourier transform of the ion count was calculated along the SWIM index n in magnitude mode. Since the sampling rate of n is 1 (in arbitrary units (a.u.)), this results in a Nyquist frequency for the encoding frequency of 0.5 (in 1/a.u.). The frequency increment is 1/64 (in 1/a.u.), since the ion count was measured over 128 data points. A quadratic fit was used for frequency-to-mass conversion using the three precursor ion *m/z* values and encoding frequencies as reference points.[46]

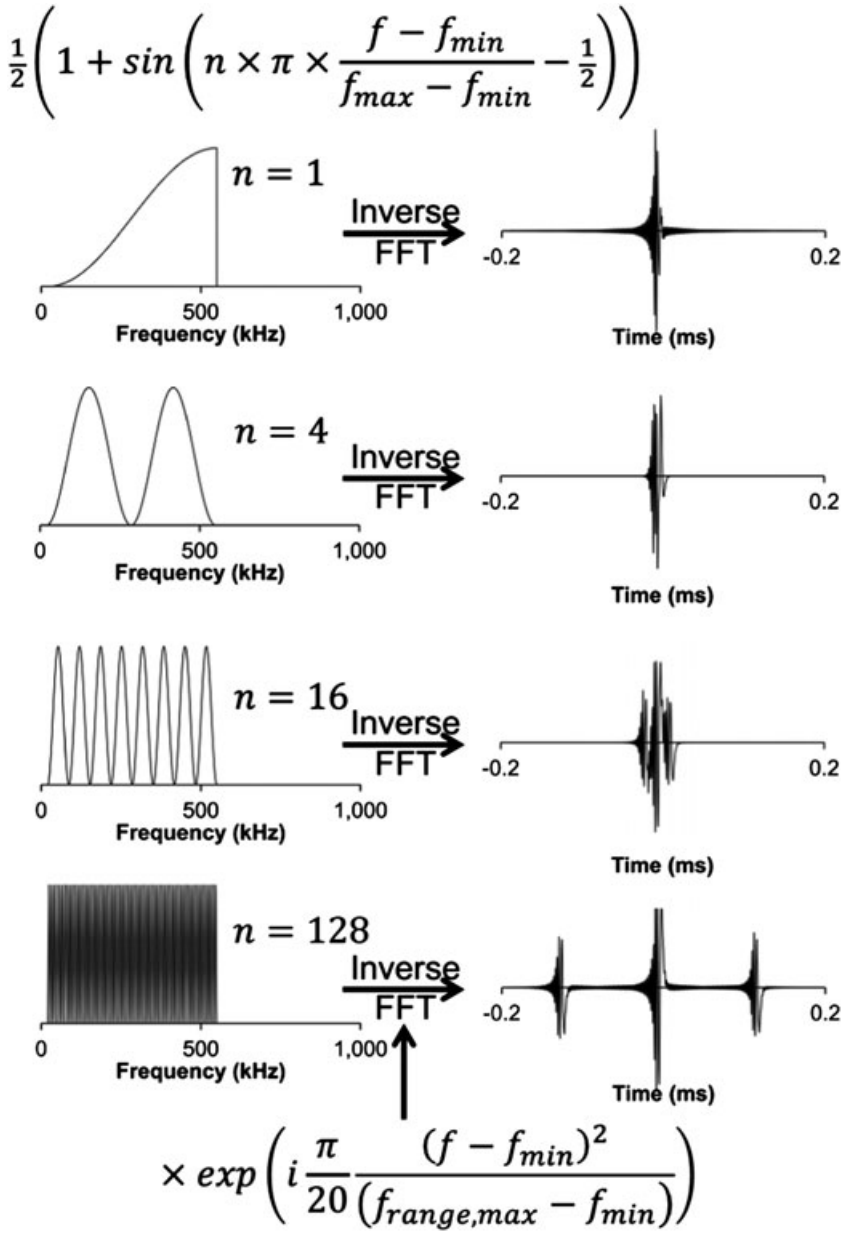

Scheme 3. Stored Waveform Ion radius Modulation. Frequency domain envelopes (left) and time-domain excitation pulses (right). Equations for the frequency domain envelopes (top) and the phase modulation (bottom).

RESULTS AND DISCUSSION

Frequencies of ion trajectories in a quadrupole are determined by the following equation:

$$f_r = \beta_r \times \frac{f_{\text{drive}}}{2} \quad (5)$$

in which f_r is the radial frequency, f_{drive} the frequency of the RF voltage applied to the quadrupole electrodes, and β_r the stability parameter used to solve the Mathieu equation in the radial dimension ($0 \leq \beta_r \leq 1$). In the area of the stability diagram generally used in mass spectrometry, the β_r stability parameter decreases when the *m/z* value increases.[41] Resonant RF voltages can be used in order to radially excite or destabilise ions of given *m/z* values in a quadrupole. Radial excitation increases with the RF amplitude and the length of the excitation voltage. This effect has been used for ion isolation in LITs by Hilger *et al.*[47] and many others.[45] In this study, hyperbolic shapes were chosen for the quadrupole rods. However, many different electrodes shapes have been developed and tested for LITs with similar results in terms of resonant frequencies. As long as resonant frequencies are stable over the size of the fragmentation zone, the quality of the radial modulation is unlikely to be affected. In each SWIM file, ions are radially excited over a range of frequencies (i.e. *m/z* values) with frequency-dependent RF amplitudes given by Eqn. (2) on the basis of the frequencies defined in Eqn. (5). For a given *m/z* value, the amplitude at their resonant

Rapid Communications in Mass Spectrometry

frequency (i.e. the radius of the ion cloud after excitation) is modulated according to the index of the SWIM file n with the following encoding frequency:

$$f_e = \frac{f_r - f_{\min}}{2(f_{\max} - f_{\min})} \quad (6)$$

in which f_e is the encoding frequency, f_r is the resonant radial frequency of the ions' trajectory, $f_{\min}$ is the minimum frequency of the frequency range (corresponding to the highest m/z value in the m/z range), and $f_{\max}$ the maximum frequency in the frequency range (corresponding to the lowest m/z value in the m/z range).

For laser-based or electron-based fragmentation methods such as IRMPD,[48] UVPD (ultraviolet photodissociation),[49] or ETD (electron transfer dissociation),[50] the zone of high fragmentation efficiency is at the centre of the quadrupole. Some fragmentation methods are pseudo-continuous (IRMPD, ETD) and some are pulsed (UVPD). When the radius of the ion cloud is large (high resonant excitation), the overlap between the ion cloud and the fragmentation zone is small, and little fragmentation can be expected. When the radius of the ion cloud is small (low resonant excitation), the overlap between the ion cloud and the fragmentation zone is high, and the fragmentation efficiency is expected to be high. Unlike in FT-ICR MS, ion manipulation in the LIT does not require ion cloud coherence.[4] As a result, CID (collisionally induced dissociation) can be used in 2D LIT MS without causing a loss of resolution.[51] The fragmentation efficiency in CID increases with ion kinetic energy: the overlap between the ion cloud and the fragmentation zone is therefore high when the ions are excited at high radius, and low when they are at low radius.

Following these hypotheses, the product ion abundances in SWIM are modulated at the same encoding frequency (defined in Eqn. (6)) as the radii of their precursors, whether the fragmentation method is laser-based, electron-based, or CID. This effect makes 2D MS in a LIT possible.

Scheme 3 shows the encoding of the ion cloud radius using SWIM, which consists of the inverse Fourier transform of a broadband excitation. If the excitation waveform has a zero phase at all frequencies, the inverse Fourier transform yields a chirp pulse resulting in a short excitation at high amplitude.[52] Chirp pulses impose high voltage amplitude (several 100 V_{pp}) and high frequency specifications on the RF amplifiers driving the mass analyser. In order to spread out the contribution of individual frequencies in excitation pulses over time and thus reduce the performance demanded of RF amplifiers, Guan *et al.* proposed an algorithm to optimise the phase modulation of a SWIFT excitation pulse for optimal amplitude reduction.[26] For broadband excitation, the optimal phase modulation is given by Eqn. (3). For broadband excitation with different amplitude envelopes, the optimal phase modulation depends on the shape of the envelope. For SWIM, this means that the optimal phase modulation function is different for each index n.

In an *in silico* experiment, there is no limitation in voltage amplitudes, but in order to adapt the 2D MS experiment to a prototype, two competing factors are in play: the voltage amplitude of the pulse and the length of the pulse. On one hand, the voltage amplitude of the pulse needs to be within the specifications of the RF amplifiers. On the other hand, compatibility of 2D MS on an LC timescale requires a limited pulse length (in the present experiment, the lowest frequency is 20 kHz, which corresponds to a pulse length of 400 µs). Furthermore, the choice of a phase modulation function that is independent of the SWIM index n leads to quicker generation of SWIM pulses before each experiment. In the present study, the phase modulation function proposed in Eqn. (3) was chosen. Figure 2 shows the peak-to-peak amplitude of each pulse with and without phase modulation for normalised frequency-domain envelopes. For all SWIM indices, the pulse with phase modulation has a lower amplitude than the pulse without phase modulation. The average amplitude is 0.187 without phase modulation, and 0.111 with phase modulation, which corresponds to an average amplitude reduction of a factor of 1.68. This nearly halves the required specifications of an RF amplifier for a 2D MS prototype.

Figure 3 shows the ion count at the end of each ion trajectory calculation as a function of SWIM index n: the total number of ions (straight lines), the number of precursor ions (crosses) and the number of product ions (full triangles). The ion trajectory calculations were performed for three m/z values: m/z 166 (Fig. 3(a)), 195 (Fig. 3(b)), and 322 (Fig. 3(c)).

Figure 3 shows that the total number of ions at the end of the simulation is modulated periodically with the index of the SWIM file. The total number of ions at the start of each simulation experiment is 100. Figures 3(a), 3(b), and 3(c) show the total number of ions at the end of each experiment, i.e. the number of ions that have not hit the electrodes during the simulation. These figures show that significant drops in the total number of ions are observed periodically. The periodic drop in total ion count corresponds to ions being excited to high radii by the SWIM pulse until they are ejected from the LIT.

The number of product ions shows the same behaviour as the total number of ions: a periodic drop from a stable number of ions (approximately 70 product ions). As the radii of the precursor ions increase, their fragmentation efficiency decreases, since the fragmentation zone is located at the centre of the LIT. This decrease in total ion count coincides with a decrease in the number of product ions: precursor ions are likely to hit the electrodes when they are excited to high

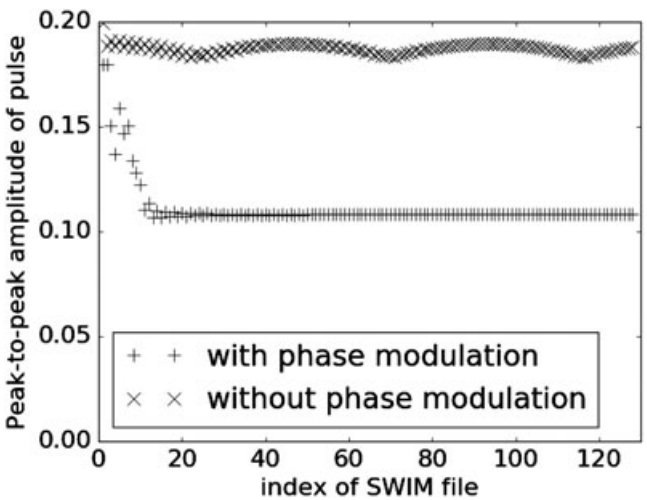

Figure 2. Peak-to-peak amplitude of SWIM pulse vs SWIM file index with and without phase modulation.

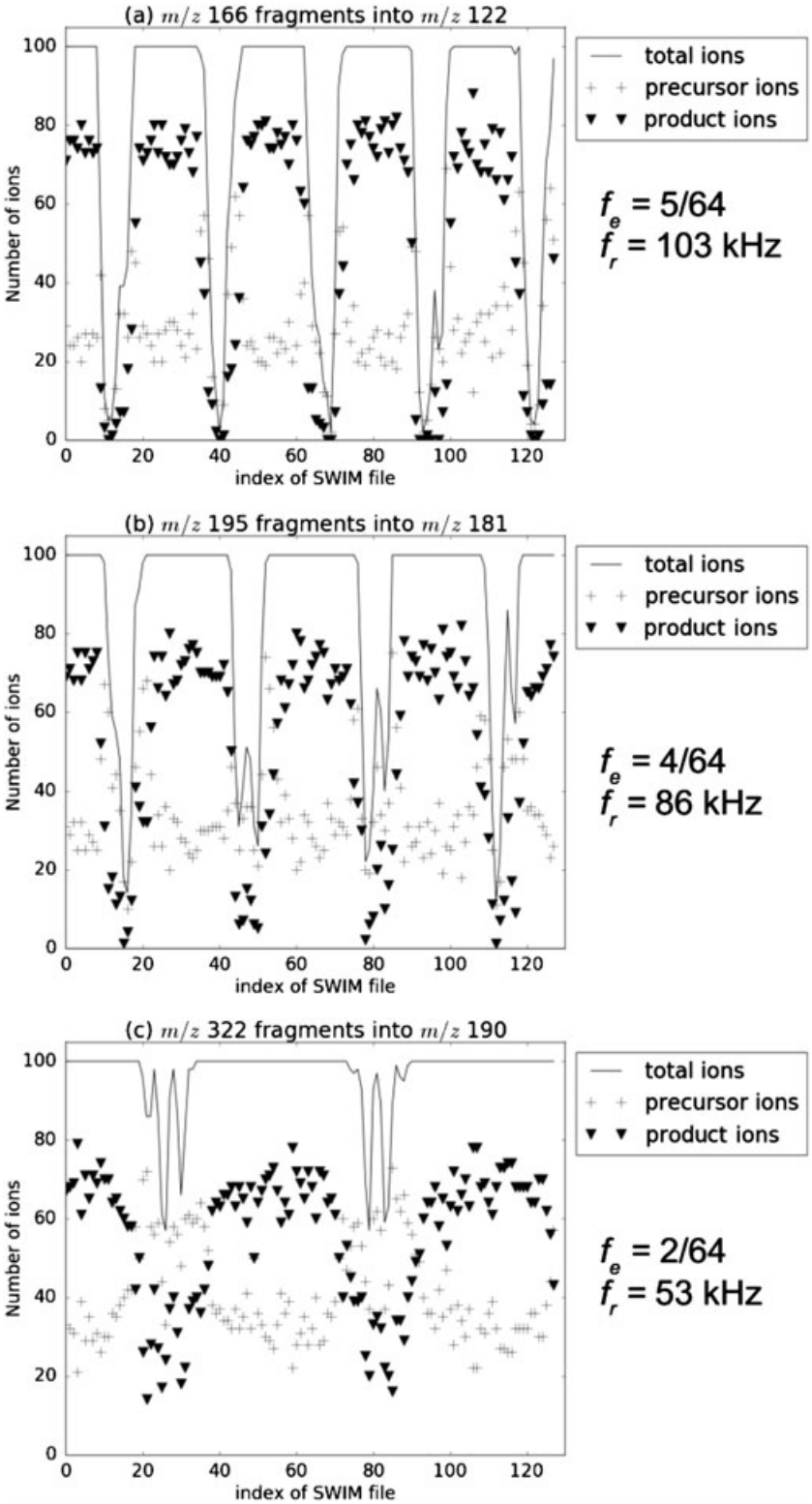

Figure 3. Total number of ions, number of precursor ions and number of product ions vs number of SWIM file for (a) *m/z* 166 fragmenting into *m/z* 122, (b) *m/z* 195 fragmenting into *m/z* 181, and (c) *m/z* 322 fragmenting into *m/z* 190.

radii (resulting in a drop in total ion number) and they are not likely to fragment because the fragmentation zone is at the centre of the LIT (resulting in a drop in the number of product ions).

The behaviour of the number of precursor ions is more complex: as the radius of precursor ions after excitation increases, their fragmentation efficiency decreases, since the precursor ions spend less time within the fragmentation zone.

Rapid Communications in Mass Spectrometry

Hence the number of precursor ions increases. When the precursor ion radius reaches the rod position within the LIT, the number of precursor ions decreases, because they are ejected from the LIT before the fragmentation period. This behaviour is not dependent on *m/z* value, as it is repeated in the experiments shown in Figs. 3(a), 3(b), and 3(c). However, the drop in total ion count at high radius increases with decreasing *m/z* value, which may be caused by the depth of the pseudopotential well, requiring higher voltage amplitudes at lower excitation frequency (i.e. higher precursor *m/z* values) to achieve the same radius.[53]

The frequency of the modulation decreases with *m/z* value: Fig. 3(a) shows that ion counts for precursors of *m/z* 166 go through five cycles, in Fig. 3(b) precursors of *m/z* 195 go through four cycles, and in Fig. 3(c) precursors of *m/z* 322 go through two cycles. These frequencies correspond to the encoding frequencies in Eqn. (6). The corresponding resonant frequencies are 103 kHz for *m/z* 166, 86 kHz for *m/z* 195 and 53 kHz for *m/z* 322. In all experiments the frequency of the ion count is the same for the precursor ions and the product ions, therefore establishing the correlation between precursor ion abundances and product ion abundances, and the possibility of 2D MS in a LIT.

Figure 4 shows the 2D mass spectrum generated with the data presented in Fig. 3. As in 2D FT-ICR mass spectra, the horizontal axis represents the *m/z* values measured at the end of the ion trajectory calculations (i.e. product *m/z* value), and the vertical axis represents the *m/z* values calculated from the frequency-to-mass conversion (i.e. precursor *m/z* value).[8] The dotted line in Fig. 4 shows the autocorrelation with a $(m/z)_{\text{precursor}} = (m/z)_{\text{product}}$ equation, corresponding to the modulation of precursor ion abundances according to their own encoding frequency (i.e. *m/z* value).

If peaks in a 2D mass spectrum can be identified by their coordinates *m/z* ($m/z_{\text{horizontal}}$, m/z_{vertical}), then Fig. 4 shows two peaks on the autocorrelation line at *m/z* (195, 195) and (322, 322). Each precursor ion has a peak on its product ion line: *m/z* (181, 195) for *m/z* 195 and *m/z* (190, 322) for *m/z* 322. The 2D mass spectrum shows a peak at *m/z* (122, 166), but no corresponding peak on the autocorrelation line at *m/z* (166, 166): the modulation of the precursor ion is double the frequency of the modulation of the product ion, because the excitation is intense enough to cause ion loss both at maximum excitation (by ejection) and at minimum excitation (by fragmentation). As a result, a peak on the autocorrelation line for *m/z* 166 is expected at *m/z* (166, 83). However, since the frequency-to-mass conversion equation in the vertical precursor is only valid over the *m/z* 166–322 range, the 2D mass spectrum does not show this peak.

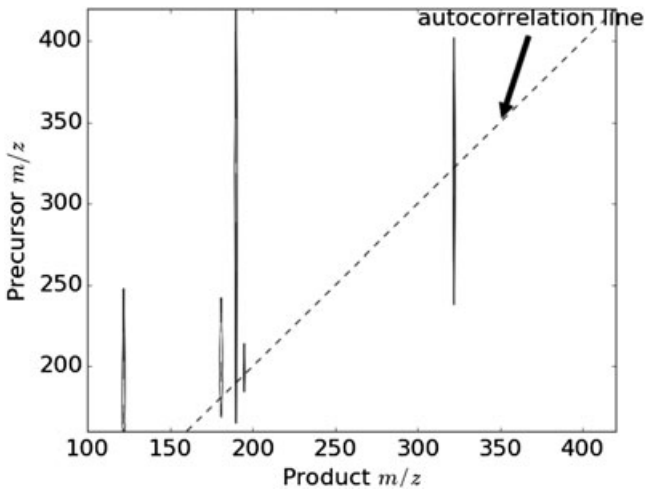

Figure 4. 2D mass spectrum generated from ion trajectory simulations in the *in silico* linear ion trap. Product ion *m/z* values are represented on the horizontal axis and precursor ion *m/z* values are represented on the vertical axis. The autocorrelation line (dotted line) shows the modulation of the abundance of the precursor ions according to their own *m/z* value.

The resolving power in the vertical precursor dimension of the 2D mass spectrum in Fig. 4 is very low: less than 10 at *m/z* 200. Increasing the number of data points along the SWIM index *n* is likely to increase the resolving power in the precursor dimension considerably, since the 2D MS method is FT-based in the precursor dimension. At present, there is no indication as to what may limit the vertical resolving power beyond the number of data points and frequency instability in the radial direction of the LIT. Similarly, the signal-to-noise ratio in the precursor dimension of the 2D mass spectrum can be expected to increase with the number of data points along the SWIM index *n* because the 2D MS method is FT-based in the precursor dimension. In the present study only 128 SWIM steps were used due to the duration of the simulations. However, physical experiments are expected to be much faster and can use 2048 SWIM steps.

In this study, unlike in 2D FT-ICR MS studies, calculating the Fourier transform of the data was only necessary in the vertical dimension, because the *m/z* values of ions were measured directly by the SIMION software. When adapting this experiment to a prototype, data processing will depend on the nature of the mass analyser. Orbitraps and FT-ICR mass spectrometers are both FT-based, which makes Fourier transforms necessary in both dimensions, but time-of-flights and quadrupoles both rely on computationally faster time-of-flight to *m/z* value conversion.

In this study, the LIT has been used as an ion manipulation device. A LIT can also be used as a mass analyser,[40] or it can be coupled with other mass analysers by transferring ions to the mass analyser at the end of the fragmentation period.[54–56] Optimising the ion transfer depends on which mass analyser is used.[57–59] Table 1 shows the characteristics of using the LIT alone as an ion manipulation device and a mass analyser compared with using the LIT in a coupling with another mass analyser. The peak capacity can be estimated by multiplying the horizontal resolving power of peaks by their vertical resolving power. In 2D FT-ICR MS, the vertical resolving power is of the order of magnitude of several hundred for 2048 data points for the t_1 increment.[8] There is no indication that using SWIM modulation in a LIT would lead to dramatically different vertical resolving powers from using the Gäumann pulse program in an ICR cell.[1] As a result, a vertical resolving power of 400 was used to estimate the peak capacities shown in Table 1.

In terms of cost, the LIT on its own or within a triple quadrupole instrument is the most attractive option, but is slow in terms of acquisition time and has a low resolving power. Coupling the LIT with an Orbitrap or an FT-ICR mass spectrometer increases the resolving power dramatically, but also the cost of the instrument. In an FT-ICR mass

Table 1. Characteristics of various mass analysers coupled with a LIT for 2D MS

Mass analyser	FT-ICR	TOF	QqQ	Orbitrap	LIT
Resolving power	400,000	10,000	3000	100,000	3000
Estimated peak capacity	160,000,000	4,000,000	1,200,000	40,000,000	1,200,000
Acquisition time (2048 scans)	>30 min	10 s	15 min	30 min	15 min
Size of datafile	50 Gb	2 Gb	0.5 Gb	50 Gb	0.5 Gb

spectrometer or an Orbitrap, the mass analysis and ion detection take about 1 s per mass spectrum, which is a major contribution to the duration of each 2D MS experiment, which requires 2048 or more mass spectra. If a LIT is coupled with a TOF mass analyser, however, the mass analysis and detection only take 10 ms. Furthermore, fast fragmentation methods such as UVPD can lead to a fragmentation period of about 10 ns. In this configuration, with 2D MS being applied to a LIT coupled with a TOF mass analyser and UVPD fragmentation, the duration of the experiment can be reduced from 1 h to 10 s, which may enable the coupling of 2D MS with online liquid or gas chromatography.

CONCLUSIONS

This study shows the feasibility of two-dimensional mass spectrometry in a linear ion trap by applying SWIM pulses to modulate the radii of precursor ion clouds before applying a radius-dependent fragmentation method. The resulting product ion abundance is modulated with the same encoding frequency as the precursor ion abundance, or half the encoding frequency of the precursor ion abundance if the maximum excitation of the precursors leads to ion ejection. Calculating the Fourier transform of ion abundances and plotting them for each *m/z* value lead to 2D mass spectra that are similar to the ones described for 2D FT-ICR MS.[8]

2D MS in a LIT can therefore be applied to various radius-dependent fragmentation techniques: laser-based (IRMPD, UVPD), electron-based (ETD, PTD),[60] or collision-based (CID). The LIT can be used both as an ion manipulation device and as a mass analyser, but can also be coupled with other mass analysers such as an FT-ICR mass spectrometer, an Orbitrap, or a TOF in order to get various desired characteristics in the experimental setup, such as high resolution or fast acquisition times. In particular, coupling the LIT with a mass analyser with a fast duty cycle can lead to acquisition times shorter than 10 s, which makes 2D MS compatible with LC or GC timescales. Such an instrument would lead to online LC/2D MS experiments in which the need for ion isolation analysis is eliminated. Online LC/2D MS would be a very useful technique for the analysis of complex samples, such as in proteomics and in petroleomics, in which MS/MS eliminates many analytes.

Acknowledgements

The authors would like to thank the Warwick Impact Fund Proof-of-Concept Award for funding this project, as well as the Engineering and Physical Sciences Research Council (Grant Nos. EP/J000302/1 and EP/N021630/1).

REFERENCES

[1] P. Pfändler, G. Bodenhausen, J. Rapin, R. Houriet, T. Gäumann. Two-dimensional Fourier transform ion cyclotron resonance mass spectrometry. *Chem. Phys. Lett.* **1987**, *138*, 195.
[2] P. Pfändler, G. Bodenhausen, J. Rapin, M. E. Walser, T. Gäumann. Broad-band two-dimensional Fourier transform ion cyclotron resonance. *J. Am. Chem. Soc.* **1988**, *110*, 5625.
[3] M. Bensimon, G. Zhao, T. Gäumann. A method to generate phase continuity in two-dimensional Fourier transform ion cyclotron resonance mass spectrometry. *Chem. Phys. Lett.* **1989**, *157*, 97.
[4] M. B. Comisarow, A. G. Marshall. Fourier transform ion cyclotron resonance spectroscopy. *Chem. Phys. Lett.* **1974**, *25*, 282.
[5] A. Kumar, R. R. Ernst, K. Wuethrich. A two-dimensional nuclear Overhauser enhancement (2D NOE) experiment for the elucidation of complete proton-proton cross-relaxation networks in biological macromolecules. *Biochem. Biophys. Res. Commun.* **1980**, *95*, 1.
[6] A. G. Marshall, T. C. L. Wang, T. L. Ricca. Ion cyclotron resonance excitation/deexcitation: a basis for stochastic Fourier transform ion cyclotron mass spectrometry. *Chem. Phys. Lett.* **1984**, *105*, 233.
[7] S. Guan, P. R. Jones. A theory for two-dimensional Fourier-transform ion cyclotron resonance mass spectrometry. *J. Chem. Phys.* **1989**, *91*, 5291.
[8] M. A. van Agthoven, M.-A. Delsuc, G. Bodenhausen, C. Rolando. Towards analytically useful two-dimensional Fourier transform ion cyclotron resonance mass spectrometry. *Anal. Bioanal. Chem.* **2013**, *405*, 51.
[9] M. A. van Agthoven, M.-A. Delsuc, C. Rolando. Two-dimensional FT-ICR/MS with IRMPD as fragmentation mode. *Int. J. Mass Spectrom.* **2011**, *306*, 196.
[10] M. A. van Agthoven, L. Chiron, M.-A. Coutouly, M.-A. Delsuc, C. Rolando. Two-dimensional ECD FT-ICR mass spectrometry of peptides and glycopeptides. *Anal. Chem.* **2012**, *84*, 5589.
[11] M. A. van Agthoven, L. Chiron, M.-A. Coutouly, A. A. Sehgal, P. Pelupessy, M.-A. Delsuc, C. Rolando. Optimization of the discrete pulse sequence for two-dimensional FT-ICR mass spectrometry using infrared multiphoton dissociation. *Int. J. Mass Spectrom.* **2014**, *370*, 114.
[12] M. A. van Agthoven, M.-A. Coutouly, C. Rolando, M.-A. Delsuc. Two-dimensional Fourier transform ion cyclotron resonance mass spectrometry: reduction of scintillation noise using Cadzow data processing. *Rapid Commun. Mass Spectrom.* **2011**, *25*, 1609.
[13] L. Chiron, M. A. van Agthoven, B. Kieffer, C. Rolando, M.-A. Delsuc. Efficient denoising algorithms for large experimental datasets and their applications in Fourier transform ion cyclotron resonance mass spectrometry. *Proc. Natl. Acad. Sci. USA* **2014**, *111*, 1385.

[14] M. A. van Agthoven, M. P. Barrow, L. Chiron, M.-A. Coutouly, D. Kilgour, C. A. Wootton, J. Wei, A. Soulby, M.-A. Delsuc, C. Rolando, P. B. O'Connor. Differentiating fragmentation pathways of cholesterol by two-dimensional Fourier transform ion cyclotron resonance mass spectrometry. *J. Am. Soc. Mass Spectrom.* **2015**, *26*, 2105.
[15] H. J. Simon, M. A. van Agthoven, P. Y. Lam, F. Floris, L. Chiron, M. A. Delsuc, C. Rolando, M. P. Barrow, P. B. O'Connor. Uncoiling collagen: a multidimensional mass spectrometry study. *Analyst* **2016**, *141*, 157.
[16] M. A. van Agthoven, C. A. Wootton, L. Chiron, M.-A. Coutouly, A. Soulby, J. Wei, M. P. Barrow, M.-A. Delsuc, C. Rolando, P. B. O'Connor. Two-dimensional mass spectrometry for proteomics, a comparative study with cytochrome c. *Anal. Chem.* **2016**, *88*, 4409.
[17] F. Floris, M. van Agthoven, L. Chiron, A. J. Soulby, C. A. Wootton, Y. P. Y. Lam, M. P. Barrow, M.-A. Delsuc, P. B. O'Connor. 2D FT-ICR MS of calmodulin: A top-down and bottom-up approach. *J. Am. Soc. Mass Spectrom.* **2016**, *27*, 1531.
[18] A. Panchaud, A. Scherl, S. A. Shaffer, P. D. von Haller, H. D. Kulasekara, S. I. Miller, D. R. Goodlett. Precursor acquisition independent from ion count: How to dive deeper into the proteomics ocean. *Anal. Chem.* **2009**, *81*, 6481.
[19] J. D. Chapman, D. R. Goodlett, C. D. Masselon. Multiplexed and data-independent tandem mass spectrometry for global proteome profiling. *Mass Spectrom. Rev.* **2014**, *33*, 452.
[20] L. C. Gillet, P. Navarro, S. Tate, H. Rost, N. Selevsek, L. Reiter, R. Bonner, R. Abersold. Targeted data extraction of the MS/MS spectra generated by data-independent acquisition: a new concept for consistent and accurate proteome analysis. *Mol. Cell. Proteomics* **2012**, *11*, O111 016717.
[21] R. S. Plumb, K. A. Johnson, P. Rainville, B. W. Smith, I. D. Wilson, J. M. Castro-Perez, J. K. Nicholson. UPLC/MSE; a new approach for generating molecular fragment information for biomarker structure elucidation. *Rapid Commun. Mass Spectrom.* **2006**, *20*, 1989.
[22] C. N. Cramer, J. M. Brown, N. Tomczyk, P. K. Nielsen, K. F. Haselmann. Electron transfer dissociation of all ions at all times, MSETD, in a quadrupole time-of-flight (Q-ToF) mass spectrometer. *J. Am. Soc. Mass Spectrom.* **2016**, ahead of print.
[23] A. G. Marshall, T. C. L. Wang, L. Chen, T. L. Ricca. New excitation and detection techniques in Fourier transform ion cyclotron resonance mass spectrometry. *ACS Symp. Ser.* **1987**, *359*, 21.
[24] T. C. L. Wang, T. L. Ricca, A. G. Marshall. Extension of dynamic range in Fourier transform ion cyclotron resonance mass spectrometry via stored waveform inverse Fourier transform excitation. *Anal. Chem.* **1986**, *58*, 2935.
[25] S. Guan, A. G. Marshall. Stored waveform inverse Fourier transform (SWIFT) ion excitation in trapped-ion mass spectrometry: theory and applications. *Int. J. Mass Spectrom. Ion Processes* **1996**, *157/158*, 5.
[26] S. Guan, R. T. McIver Jr. Optimal phase modulation in stored wave form inverse Fourier transform excitation for Fourier transform mass spectrometry. I. Basic algorithm. *J. Chem. Phys.* **1990**, *92*, 5841.
[27] P. B. O'Connor, F. W. McLafferty. High-resolution ion isolation with the ion cyclotron resonance capacitively coupled open cell. *J. Am. Soc. Mass Spectrom.* **1995**, *6*, 533.
[28] P. B. O'Connor, D. P. Little, F. W. McLafferty. Isotopic assignment in large-molecule mass spectra by fragmentation of a selected isotopic peak. *Anal. Chem.* **1996**, *68*, 542.
[29] F. W. McLafferty, D. B. Stauffer, S. Y. Loh, E. R. Williams. Hadamard transform and "no-peak" enhancement in measurement of tandem Fourier transform mass spectra. *Anal. Chem.* **1987**, *59*, 2212.
[30] E. R. Williams, S. Y. Loh, F. W. McLafferty, R. B. Cody. Hadamard transform measurement of tandem Fourier-transform mass spectra. *Anal. Chem.* **1990**, *62*, 698.
[31] X. Gao, T. D. Wood. Sources of negative peaks in Hadamard transform/Fourier transform mass spectrometry/mass spectrometry. *Rapid Commun. Mass Spectrom.* **1996**, *10*, 1997.
[32] S. Haebel, T. Gäumann. Difference measurements and shaped waveforms applied to Hadamard transform FT/ICR. *Int. J. Mass Spectrom. Ion Processes* **1995**, *144*, 139.
[33] C. W. Ross, III, S. Guan, P. B. Grosshans, T. L. Ricca, A. G. Marshall. Two-dimensional Fourier transform ion cyclotron resonance mass spectrometry/mass spectrometry with stored-waveform ion radius modulation. *J. Am. Chem. Soc.* **1993**, *115*, 7854.
[34] M. V. Gorshkov, E. N. Nikolaev. Optimal cyclotron radius for high resolution FT-ICR spectrometry. *Int. J. Mass Spectrom. Ion Processes* **1993**, *125*, 1.
[35] G. van der Rest, A. G. Marshall. Noise analysis for 2D tandem Fourier transform ion cyclotron resonance mass spectrometry. *Int. J. Mass Spectrom.* **2001**, *210/211*, 101.
[36] C. W. Ross, W. J. Simonsick Jr, D. J. Aaserud. Application of stored waveform ion modulation 2D-FTICR MS/MS to the analysis of complex mixtures. *Anal. Chem.* **2002**, *74*, 4625.
[37] O.-K. Yoon, R. N. Zare. (Leland Stanford Junior University, USA). Method of making gate for charged particle motion. *US Patent 7448131*, **2008**.
[38] J. Wilson, R. W. Vachet. Multiplexed MS/MS in a quadrupole ion trap mass spectrometer. *Anal. Chem.* **2004**, *76*, 7346.
[39] A. M. Graichen, R. W. Vachet. Multiplexed MS/MS in a miniature rectilinear ion trap. *J. Am. Soc. Mass Spectrom.* **2011**, *22*, 683.
[40] J. C. Schwartz, M. W. Senko, J. E. P. Syka. A two-dimensional quadrupole ion trap mass spectrometer. *J. Am. Soc. Mass Spectrom.* **2002**, *13*, 659.
[41] R. E. March. An introduction to quadrupole ion trap mass spectrometry. *J. Mass Spectrom.* **1997**, *32*, 351.
[42] B. A. Collings, W. R. Stott, F. A. Londry. Resonant excitation in a low-pressure linear ion trap. *J. Am. Soc. Mass Spectrom.* **2003**, *14*, 622.
[43] D. J. Douglas, N. V. Konenkov. Mass selectivity of dipolar resonant excitation in a linear quadrupole ion trap. *Rapid Commun. Mass Spectrom.* **2014**, *28*, 430.
[44] R. K. Julian, Jr., R. G. Cooks. Broad-band excitation in the quadrupole ion trap mass spectrometer using shaped pulses created with the inverse Fourier transform. *Anal. Chem.* **1993**, *65*, 1827.
[45] A. V. Mordehai, J. D. Henion. Computer-designed waveform technique for reducing chemical noise in atmospheric-pressure ionization/ion-trap mass spectrometry. *Rapid Commun. Mass Spectrom.* **1993**, *7*, 1131.
[46] E. B. Ledford, Jr, D. L. Rempel, M. L. Gross. Space charge effects in Fourier transform mass spectrometry. II. Mass calibration. *Anal. Chem.* **1984**, *56*, 2744.
[47] R. T. Hilger, R. E. Santini, C. A. Luongo, B. M. Prentice, S. A. McLuckey. A method for isolating ions in quadrupole ion traps using an excitation waveform generated by frequency modulation and mixing. *Int. J. Mass Spectrom.* **2015**, *377*, 329.
[48] S. A. Hofstadler, K. A. Sannes-Lowery, R. H. Griffey. Infrared multiphoton dissociation in an external ion reservoir. *Anal. Chem.* **1999**, *71*, 2067.
[49] J. R. Cannon, M. B. Cammarata, S. A. Robotham, V. C. Cotham, J. B. Shaw, R. T. Fellers, B. P. Early, P. M. Thomas, N. L. Kelleher, J. S. Brodbelt. Ultraviolet photodissociation for characterization of whole proteins on a chromatographic time scale. *Anal. Chem.* **2014**, *86*, 2185.

[50] G. C. McAlister, D. Phanstiel, D. M. Good, W. T. Berggren, J. J. Coon. Implementation of electron-transfer dissociation on a hybrid linear ion trap-orbitrap mass spectrometer. *Anal. Chem.* **2007**, *79*, 3525.
[51] A. G. Marshall, C. L. Hendrickson, G. S. Jackson. Fourier transform ion cyclotron resonance mass spectrometry: a primer. *Mass. Spectrom. Rev.* **1998**, *17*, 1.
[52] A. G. Marshall, T. C. L. Wang, T. L. Ricca. Tailored excitation for Fourier transform ion cyclotron mass spectrometry. *J. Am. Chem. Soc.* **1985**, *107*, 7893.
[53] D. Gerlich. Inhomogeneous RF fields: a versatile tool for the study of processes with slow ions. *Adv. Chem. Phys.* **1992**, *82*, 1.
[54] Y. Hashimoto, H. Hasegawa, H. Satake, T. Baba, I. Waki. Duty cycle enhancement of an orthogonal acceleration TOF mass spectrometer using an axially-resonant excitation linear ion trap. *J. Am. Soc. Mass Spectrom.* **2006**, *17*, 1669.
[55] A. Makarov, E. Denisov, O. Lange, S. Horning. Dynamic range of mass accuracy in LTQ Orbitrap hybrid mass spectrometer. *J. Am. Soc. Mass Spectrom.* **2006**, *17*, 977.
[56] G. Hopfgartner, E. Varesio, V. Tschaeppaet, C. Grivet, E. Bourgogne, L. A. Leuthold. Triple quadrupole linear ion trap mass spectrometer for the analysis of small molecules and macromolecules. *J. Mass Spectrom.* **2004**, *39*, 845.
[57] M. A. van Agthoven, P. Colomby, M. Surugue, C. Beaugrand, F. L. Wind, J.-C. Tabet. Ion kinetic energy measurements in two soft ion ejection methods from a quadrupole ion trap. *Int. J. Mass Spectrom.* **2010**, *296*, 59.
[58] F. A. Londry, J. W. Hager. Mass selective axial ion ejection from a linear quadrupole ion trap. *J. Am. Soc. Mass Spectrom.* **2003**, *14*, 1130.
[59] B. E. Wilcox, C. L. Hendrickson, A. G. Marshall. Improved ion extraction from a linear octopole ion trap: SIMION analysis and experimental demonstration. *J. Am. Soc. Mass Spectrom.* **2002**, *13*, 1304.
[60] J. Martens, G. Berden, J. Oomens. Structures of fluoranthene reagent anions used in electron transfer dissociation and proton transfer reaction tandem mass spectrometry. *Anal. Chem.* **2016**, *88*, 6126.

SUPPORTING INFORMATION

Additional Supporting Information may be found online in the supporting information tab for this article.

